J Mater Sci (2019) 54:2271–2277

Computation

Lightweight AlCrTiV high-entropy alloys with dual-phase microstructure via microalloying

Xuejun Huang[1], Jiashi Miao[1], and Alan A. Luo[1,2,*]

[1] Department of Materials Science and Engineering, The Ohio State University, Columbus, OH 43210, USA
[2] Department of Integrated Systems Engineering, The Ohio State University, Columbus, OH 43210, USA

Received: 16 July 2018
Accepted: 24 September 2018
Published online: 1 October 2018

ABSTRACT

Single-phase equiatomic AlCrTiV high-entropy alloy has high hardness and relative low density. Further hardness increase was achieved through the addition of lightweight microalloying elements, based on calculation of phase diagram (CALPHAD) modeling. According to the results of CALPHAD calculation, microalloying equiatomic AlCrTiV high-entropy alloy with boron, carbon, and silicon will result in the formation of secondary phases. CALPHAD calculation also shows addition of lightweight elements can affect the order–disorder transition of microalloyed AlCrTiV high-entropy alloy. Dual-phase microstructure consisting of BCC_B2 matrix and an intermetallic phase is observed in these microalloyed alloys. Electron microscopy characterization confirms that the experimental results are consistent with CALPHAD prediction. Microalloyed AlCrTiV alloys have density close to 4.5 g cm^{-3} and hardness up to 710 HV. Compared to other high-entropy alloys, the microalloyed AlCrTiV alloys have a good combination of specific hardness, low cost, and ease of manufacturing, and thus they are promising for lightweight applications.

Introduction

The concept of "high-entropy alloys" (HEAs), also called "multi-principal element" (MPE) alloys, has opened up vast composition spaces for developing new alloys. The transition metal HEAs, such as CoCrFeMnNi and its variants, have been under extensive investigations since they were first discovered in 2004 [1–7]. One outstanding property of CoCrFeMnNi HEAs, as well as medium-entropy alloys consisting of a subset of five elements, is their exceptional toughness at cryogenic temperatures, which is superior to any existing metallic materials [2, 8]. Recently, another group of HEAs based on refractory elements, such as TaNbHfZrTi [9, 10] and WNbMoTaV [11], also attracted increasing attentions. Refractory HEAs exhibit both good high-temperature stability and mechanical properties, some of which are comparable to those of superalloys. Although these HEAs exhibit some extraordinary properties, one common drawback is their high density, which greatly limits their applications in the transportation sectors where lightweighting is critical.

Address correspondence to E-mail: luo.445@osu.edu

https://doi.org/10.1007/s10853-018-2970-4

The original motivation to design a high-entropy alloy by mixing many (at least more than five) different elements is to maximize the ideal configuration entropy and further to favor the formation of single-phase solid solution [12]. However, further research has demonstrated that the high ideal configurational entropy is not sufficient to stabilize solid solution phases [13]. The enthalpy of mixing also plays an important role in determining the stability of solid solution phases and intermetallic phases. As a matter of fact, if one pair of elements have strong tendency to form intermetallic in their binary system, the HEAs containing this pair of elements are also prone to the formation of intermetallics [13]. Therefore, in order to form a single-phase solid solution by mixing multiple elements, each pair of them must have relatively large solubility in their binary system [14]. Examining the binary phase diagrams of the elements in the first three rows of the periodic table and considering the criterion of low density, we chose the AlCrTiV quaternary system as a candidate for lightweight HEA development. Both Ti–V and Cr–V are completely miscible to each other [15]. Ti–Cr also forms a solid solution across whole composition range at elevated temperatures. Although Al can form aluminide with the other three elements, it has very large solubility in Ti, Cr and V. Based on CALculation of PHAse Diagrams (CALPHAD) modeling, a large body-centered cubic (BCC) single-phase region was predicted in AlCrTiV quaternary system [16] and was later confirmed [17]. Further experimental study shows that the BCC phase in fact has an ordered BCC_B2 structure at low temperature [17].

In previous research of HEAs, a single-phase solid solution microstructure was preferred, and the formation of intermetallic phases was avoided to maximize the configuration entropy, thus improving strength [18] However, in conventional alloy design, intermetallic phases are deliberately introduced to achieve significant property improvement by taking advantage of secondary phase strengthening. Recently, same strengthening strategy was introduced in designing high-entropy alloys [19, 20]. It was also reported the addition of metallic alloying elements, such as nonmetallic elements boron [21] and carbon [22], resulted in the formation of intermetallic phases and significantly increased the hardness of the base HEAs.

In this work, AlCrTiV-based lightweight high-entropy alloys were designed using a CALPHAD-based approach, followed by experimental validation. Previous research shows that CALPHAD modeling is valid for predicting the phase constitution in HEAs prepared by casting method [23]. The equiatomic AlCrTiV-based alloy was microalloyed with nonmetallic elements including boron (B), carbon (C) and silicon (Si). These lighter alloying elements were selected to further reduce the density of HEAs and form secondary intermetallic phases to increase the hardness. As compared with other HEAs, the newly developed microalloyed AlCrTiV HEAs have excellent hardness up to 710 HV and low density close to 4.5 g cm^{-3}.

Methods

The phase constitution of HEA systems was predicted using the Thermo-Calc software package. Equilibrium phase diagrams were calculated using TCHEA2 database for $(AlCrTiV)_{100-x}C_x$ and $(AlCrTiV)_{100-x}Si_x$. Since boron is not included in TCHEA2 database, database TCTI1 was instead adopted for $(AlCrTiV)_{100-x}B_x$. Based on the CALPHAD results, HEA samples were prepared by arc-melting under a high-purity argon atmosphere. The purity of raw materials is at least 99.9%. Each sample was remelted for five times to ensure homogeneity. The samples for microstructure characterization were cut from as-cast ingots using a low-speed diamond saw. The cut specimens were mounted, mechanically ground, and polished following the procedures of conventional metallographic specimen preparation. Scanning electron microscope (SEM) characterization was conducted using a FEI Apreo SEM. Thin-foil transmission electron microscopy (TEM) specimens were prepared using lift-out techniques on a Helios NanoLab 600 dual-beam focused ion beam (FIB)—SEM system. Ion damage induced during preparation of lift-out TEM specimens were cleaned using a Fischione 1040 nanomill before TEM observation. TEM investigation was carried out on a FEI Tecnai TF20 TEM-STEM (scanning transmission electron microscopy) operating under 200 keV. Hardness test was performed on a LECO LM100AT microhardness tester using a load of 200 g and dwell time of 15 s. At least 10 points were tested on each sample to calculate average hardness values. All samples were investigated in as-cast condition.

Results and discussion

Figure 1 shows the pseudo-binary phase diagrams of AlCrTiV–B/C/Si with the content of microalloying elements up to 10 at.%. Except that Si has the maximum solubility of 1 at.% in AlCrTiV, B and C have almost zero solubility in the base alloy. Based on the CALPHAD prediction in Fig. 1a, small additions of B result in a dual-phase region of BCC+TiB beneath the solidus line. As more B is added, Ti_3B_4 phase starts to form. When the B content is above 3.6 at.%, Ti_3B_4 will first solidify from liquid. The stability of Ti_3B_4 outcompetes TiB as the temperature decreases. Below about 720 °C, there is only Ti_3B_4 intermetallic left. The phase constitution in AlCrTiV–C is relatively simple as shown in Fig. 1b. Carbon additions lead to a dual-phase region, BCC + TiC, which extends up to 10 at.% of C addition. A pseudo-eutectic point is observed at 2.6 at.% of C and 1782 °C. At hypereutectic compositions, TiC first would solidify from the liquid. The phase diagram of AlCrTiV–Si is very similar to that of AlCrTiV–C. Ti_5Si_3 forms when Si content is above the solubility limit. There is also a pseudo-eutectic point in AlCrTiV–Si phase diagram at 7.2 at.% of Si and 1710 °C. When the composition of Si is beyond the eutectic point, Ti_5Si_3 solidifies first. In all three phase diagrams, a transition from disordered BCC_A2 phase to ordered BCC_B2 phase is predicted by CALPHAD as temperature decreases, which is illustrated by the dashed line. This prediction agrees with previous research [16]. The additions of light elements have different effects on the order–disorder transition temperatures. Based on the CALPHAD calculations, C can decrease the transition temperature while Si increases the transition temperature. However, B does not significantly change the order-disorder transition. The CALPHAD result predicts that BCC_A2 only partially transfers to BCC_B2 in AlCrTiV–B system below the transition line; whereas in AlCrTiV-C/Si systems, BCC_A2 completely transfers to BCC_B2. Because these transitions happen at high temperatures, they may not be observed in as-cast condition or at room temperature.

Based on the above CALPHAD results, four microalloyed HEAs were prepared for each alloying element at compositions of 0.5 at.%, 1.5 at.%, 2.5 at.%, and 5 at.%. The equiatomic AlCrTiV-based alloy was also prepared for comparison. Figure 2a–c shows the as-cast microstructure of AlCrTiV alloys with additions of 5 at.% of B, C, and Si, respectively. It can be seen that, in all three alloys, dual-phase microstructure forms due to the additions of microalloying elements. The bright area is the AlCrTiV matrix, and the dark phases are intermetallics. The crystal structure of secondary phases in these alloys was identified using electron diffraction methods. Figure 3 shows bright-field STEM images, as well as selected area diffraction patterns (SADP), of an as-cast AlCrTiV sample and three microalloyed samples.

The SADP insert in Fig. 3a shows that the as-cast equiatomic AlCrTiV sample is of a single phase with a crystal structure of BCC_B2. The matrix phase of other three microalloyed samples has the same BCC_B2 crystal structure as that of the equiatomic AlCrTiV sample. With B addition, TEM diffraction study shows that the secondary phase in the specimen is TiB phase with an orthorhombic crystal structure. Figure 2a shows that TiB phase is present with needle-like morphology at 5 at.% of B. Although

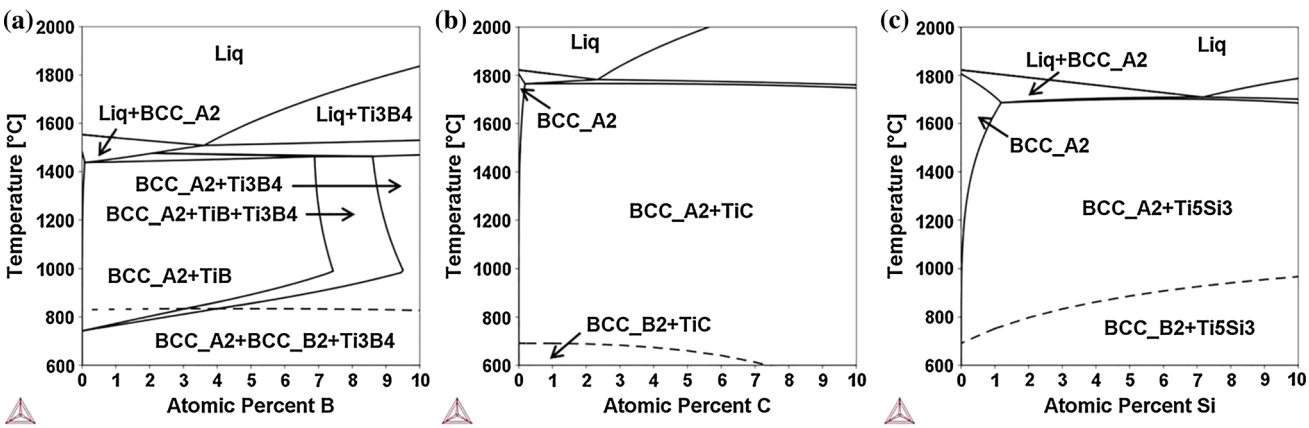

Figure 1 Pseudo-binary phase diagram of **a** AlCrTiV–B, **b** AlCrTiV–C, and **c** AlCrTiV–Si systems.

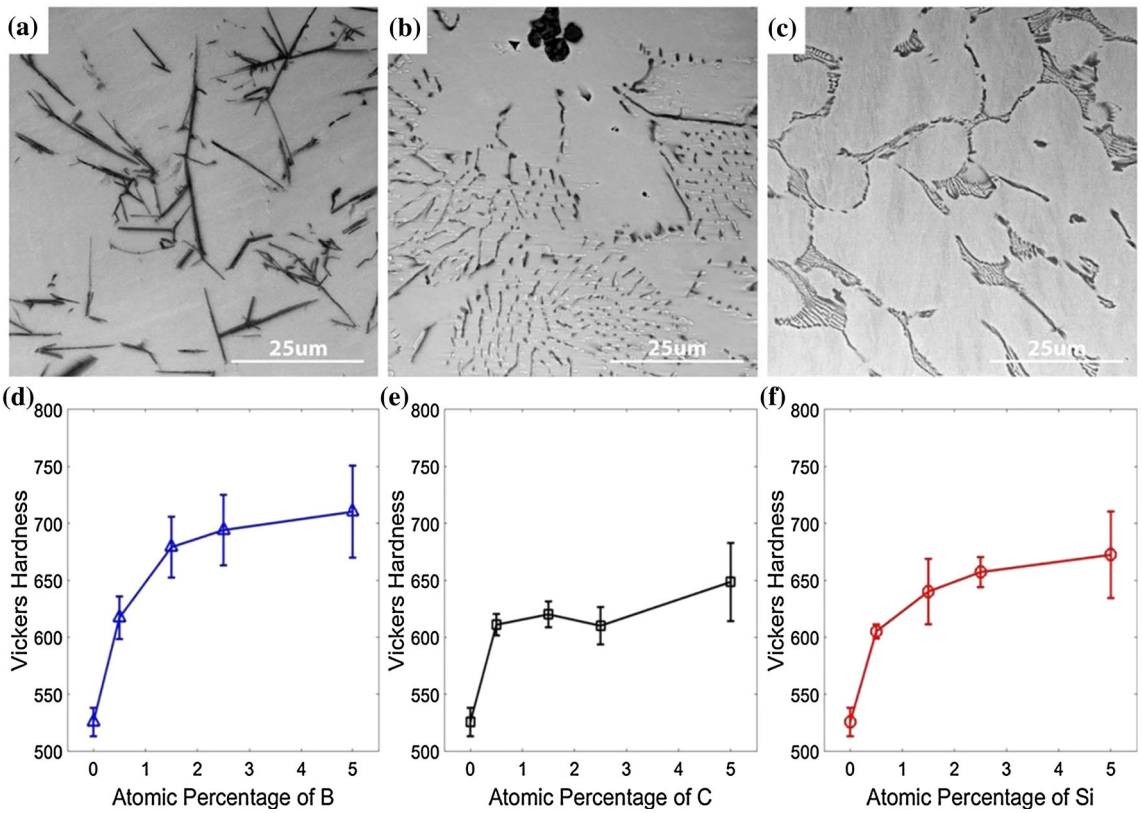

Figure 2 SEM charatcreization of the microstructure of as-cast microalloyed AlCrTiV specimens, **a** $(AlCrTiV)_{95}B_5$, **b** $(AlCrTiV)_{95}C_5$, and **c** $(AlCrTiV)_{95}Si_5$; and measured hardness values, **d** $(AlCrTiV)_{100-x}B_x$, **e** $(AlCrTiV)_{100-x}C_x$, and **f** $(AlCrTiV)_{100-x}Si_x$.

primary Ti_3B_4 phase is predicted to form when B content is larger than 3.6 at.%, there is no Ti_3B_4 observed in the specimen. It is possible that CALPHAD overestimates the stability of Ti_3B_4 phase. The TCTI1 database used to predict AlCrTiV–B pseudo-binary phase diagram is designed for Ti-rich corner of composition space and is not optimized for HEA systems. The secondary phase in $(AlCrTiV)_{100-x}C_x$ is identified as TiC as shown in Fig. 3c. The $(AlCrTiV)_{95}C_5$ sample, Fig. 2b, demonstrates the unique feature of eutectic microstructure, alternating laths of matrix and secondary phase. Other $(AlCrTiV)_{100-x}C_x$ samples share the same feature but with lower volume fractions of eutectic phase as C content decreases. These observations agree well with the calculated phase diagram in Fig. 1b. In addition, there is a coarse TiC particle present in Fig. 3b, which is the primary TiC. The coarse primary TiC phase is not observed in other $(AlCrTiV)_{100-x}C_x$ samples with low C additions. This demonstrates that the eutectic point is between 2.5 at.% and 5 at.% of C, and the predicted eutectic point in Fig. 1b falls right in this range. Figure 3d shows the diffraction pattern of Ti_5Si_3 phase in $(AlCrTiV)_{100-x}Si_x$ alloys. The eutectic microstructure is also obvious in $(AlCrTiV)_{100-x}Si_x$ samples, except the one with 0.5 at.% Si addition. There is no secondary phase forming in $(AlCrTiV)_{99.5}Si_{0.5}$, which is in good agreement with the CALPHAD results. The calculated phase diagram, Fig. 1c, shows that Si is soluble in AlCrTiV-based alloy up to 1 at.% addition. According to CALPHAD calculations, the highest amount of Si addition is still below the predicted eutectic composition, and there is no primary Ti_5Si_3 phase found in all samples. Overall, CALPHAD modeling successfully predicted the phase constitution and microstructure of AlCrTiV HEAs microalloyed with B, C, and Si. For the one alloyed with B, CALPHAD overestimates the stability of Ti_3B_4 phase.

Figure 2d–f summarizes the change of hardness of alloys with the increase in the content of lightweight alloying elements. For all three microalloying elements, the hardness value changes in the same trend. Only 0.5 at.% addition of alloying elements result in significant increases in hardness. As the alloying additions further increase, the hardness values

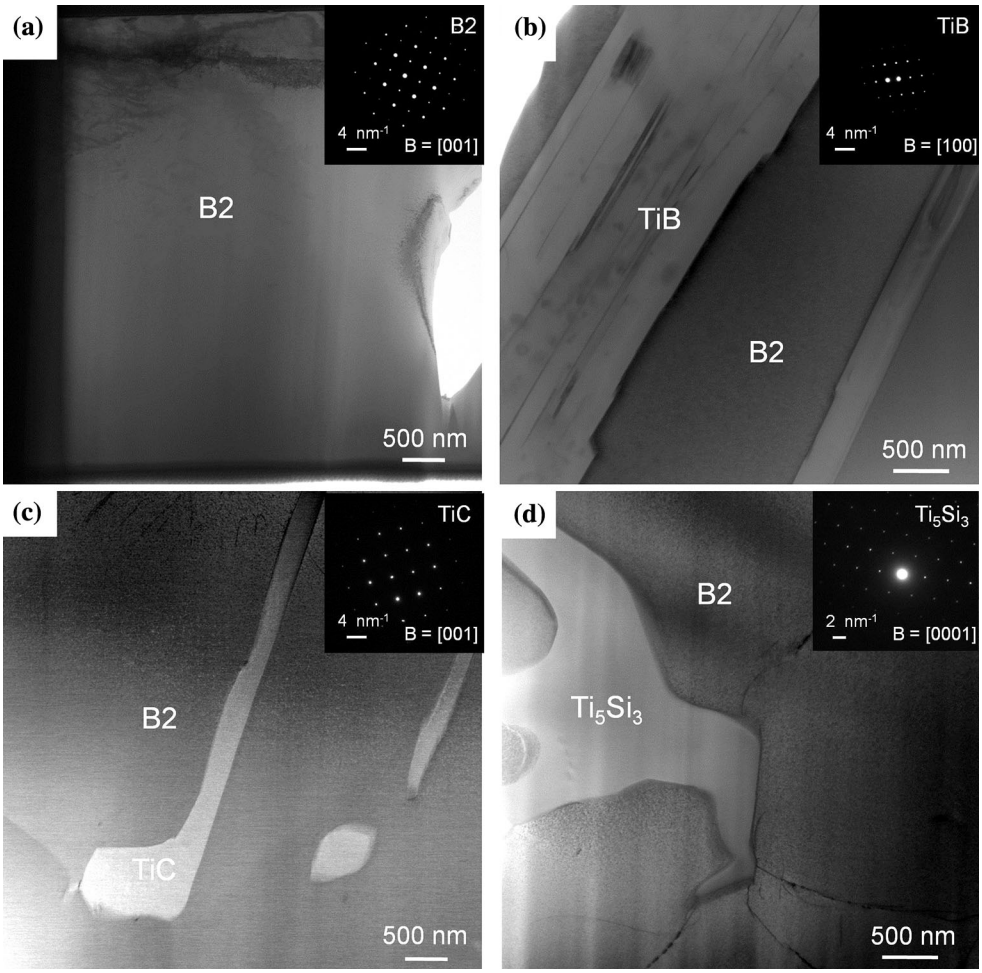

Figure 3 TEM/STEM characterization of as-cast AlCrTiV and microalloyed AlCrTiV alloys: **a** bright-field STEM image with an inset selected area diffraction pattern of B2 phase, **b** bright-field STEM image of $(AlCrTiV)_{95}B_5$ with an inset diffraction pattern of TiB, **c** bright-field STEM image of $(AlCrTiV)_{95.5}C_{0.5}$ with a inset diffraction pattern of TiC, and **d** field STEM image of $(AlCrTiV)_{95.5}Si_{0.5}$, with a inset diffraction pattern of Ti5Si3.

slowly climb and level off. The hardness increases should be attributed to the introduction of hard secondary phases with one exception, $(AlCrTiV)_{99.5}Si_{0.5}$. Since no intermetallic phase is observed in $(AlCrTiV)_{99.5}Si_{0.5}$ sample, solid solution strengthening contributes its hardness increase. In general, the hardness is proportional to the volume fraction of the intermetallic phases. With 5 at.% additions of B, C, and Si, the highest hardness is reached for $(AlCrTiV)_{100-x}B_x$ alloys at 710 HV; for $(AlCrTiV)_{100-x}C_x$ and $(AlCrTiV)_{100-x}Si_x$ alloys, the highest hardness is 642 HV and 679 HV, respectively. All microalloyed AlCrTiV alloys have hardness above 600 HV, which is more than 20% improvement compared to the base alloy. This proves that "dual-phase" microstructure is an effective way to engineer HEAs. Among three alloying elements, B is the most potent one in increasing the hardness of the AlCrTiV-based alloy.

Figure 4 is a plot of specific hardness (hardness/density) versus density of reported bulk lightweight HEAs [16, 24–31]. The density of HEAs is calculated theoretically using the following equation based on the "rule of mixture":

$$\rho = \frac{\sum x_i M_i}{\sum x_i V_i}$$

where M_i and V_i is the molar weight and molar volume of element i respectively, and x_i is the corresponding molar fraction. The density of microalloyed AlCrTiV-based alloys is between 4.7 and 4.9 g cm^{-3}. For the convenience of comparison, all hardness values are converted to the unit of GPa. It is

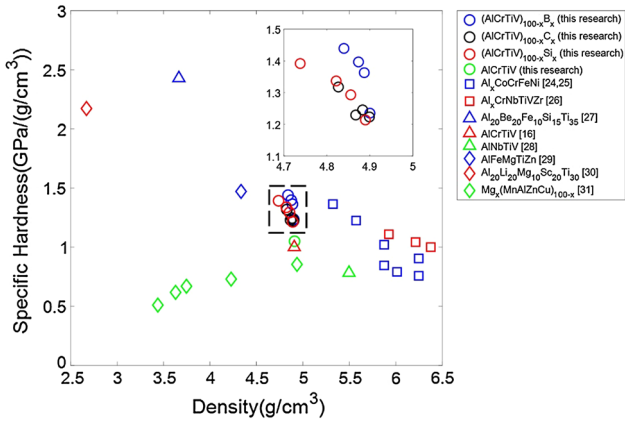

Figure 4 Comparison of hardness and density of reported lightweight HEAs.

common to add Al to existing CoCrFeMnNi based HEAs to lower their density, such as $Al_xCoCrFeNi$ [24, 25] and $Al_xCrNbTiVZr$ [26]. Although these alloys have the hardness comparable with microalloyed AlCrTiV alloys, their density is much higher. In order to making HEAs with density lower than 4.5 g cm^{-3}, it is inevitable to use alkali and alkaline earth metals, such as Li and Mg [27, 30, 31]. However, these elements pose considerable challenges to alloying processes and component manufacturing. For example, HEAs containing Li and Mg are usually produced by mechanical alloying, which is expensive for industrial scale production. In Fig. 4, the desired materials should be located at the top left corner, with low density and high hardness. Two alloys are in this region: $Al_{20}Be_{20}Fe_{10}Si_{15}Ti_{35}$ contains toxic and expensive Be; and $Al_{20}Li_{20}Mg_{10}Sc_{20}Ti_{30}$ contains Li and Sc which are both expensive and difficult to alloy. Despite the slightly lower specific hardness, the microalloyed AlCrTiV HEAs in this study contain less expensive alloying elements. Therefore, among all current available lightweight HEAs, the microalloyed AlCrTiV alloys offer more balanced properties, low cost, and ease of manufacturing.

In summary, microalloyed lightweight equiatomic AlCrTiV alloys with dual-phase microstructure through the addition of nonmetallic alloying element including B, C, and Si were designed using CALPHAD approach. The main constitution phases in AlCrTiV-based alloys predicted by CALPHAD methods match with experimental results, except for overestimating the stability of Ti_3B_4 phase in alloys microalloyed with B. CALPHAD predicts that adding C and Si can decrease and increase the order-disorder transition temperature, respectively; while adding B has no obvious effect on it. As compared with single-phase AlCrTiV-based alloy, all microalloyed AlCrTiV alloys have improved hardness and reduced density close to 4.5 g cm^{-3}. Among three alloying elements, B is the most effective one in increasing hardness of AlCrTiV alloys. With an addition of 5 at% B, a hardness of 710 HV can be achieved. Compared to other bulk lightweight HEAs, microalloyed AlCrTiV HEAs have a good combination of density and hardness and the advantage of easy processing.

Acknowledgements

The authors wish to acknowledge the financial support from The Ohio State University (OSU) and helpful discussions with Dr. Weihua Sun, a former postdoctoral researcher at OSU.

References

[1] Cantor B, Chang ITH, Knight P, Vincent AJB (2004) Microstructural development in equiatomic multicomponent alloys. Mater Sci Eng A 375–377:213–218

[2] Gludovatz B, Hohenwarter A, Catoor D et al (2014) A fracture-resistant high-entropy alloy for cryogenic applications. Science (80-) 345:1153–1158

[3] Otto F, Dlouhý A, Somsen C et al (2013) The influences of temperature and microstructure on the tensile properties of a CoCrFeMnNi high-entropy alloy. Acta Mater 61:5743–5755

[4] Miao J, Slone CE, Smith TM et al (2017) The evolution of the deformation substructure in a Ni–Co–Cr equiatomic solid solution alloy. Acta Mater 132:35–48

[5] Pickering EJ, Muñoz-Moreno R, Stone HJ, Jones NG (2016) Precipitation in the equiatomic high-entropy alloy CrMnFeCoNi. Scr Mater 113:106–109

[6] He F, Wang Z, Wu Q et al (2017) Phase separation of metastable CoCrFeNi high entropy alloy at intermediate temperatures. Scr Mater 126:15–19

[7] Otto F, Dlouhý A, Pradeep KG et al (2016) Decomposition of the single-phase high-entropy alloy CrMnFeCoNi after prolonged anneals at intermediate temperatures. Acta Mater 112:40–52

[8] Miao J, Slone CE, Smith TM et al (2017) The evolution of the deformation substructure in a Ni–Co–Cr equiatomic solid solution alloy. Acta Mater 132:35–48

[9] Senkov ON, Scott JM, Senkova SV et al (2011) Microstructure and room temperature properties of a high-entropy TaNbHfZrTi alloy. J Alloys Compd 509:6043–6048

[10] Senkov ON, Scott JM, Senkova SV et al (2012) Microstructure and elevated temperature properties of a refractory TaNbHfZrTi alloy. J Mater Sci 47:4062–4074. https://doi.org/10.1007/s10853-012-6260-2

[11] Senkov ON, Wilks GB, Scott JM, Miracle DB (2011) Mechanical properties of Nb 25Mo25Ta25W25 and V20Nb20Mo20Ta20W20. Intermetallics 19:698–706

[12] Yeh JW, Chen SK, Lin SJ et al (2004) Nanostructured high-entropy alloys with multiple principal elements: novel alloy design concepts and outcomes. Adv Eng Mater 6:299–303

[13] Otto F, Yang Y, Bei H, George EP (2013) Relative effects of enthalpy and entropy on the phase stability of equiatomic high-entropy alloys. Acta Mater 61:2628–2638

[14] Pradeep KG, Wanderka N, Choi P et al (2013) Atomic-scale compositional characterization of a nanocrystalline AlCrCuFeNiZn high-entropy alloy using atom probe tomography. Acta Mater 61:4696–4706

[15] Villars P, Okamoto H, Cenzual K (2016) ASM alloy phase diagram database. ASM International, Materials Park, OH

[16] Luo AA, Sun W, Huang X (2016) High-entropy AlCrTiV alloys. US Patent 62/415691

[17] Qiu Y, Hu YJ, Taylor A et al (2017) A lightweight single-phase AlTiVCr compositionally complex alloy. Acta Mater 123:115–124

[18] Murty BS, Yeh JW, Ranganathan S (2014) High-entropy alloys. Butterworth-Heinemann, Oxford

[19] Gwalani B, Soni V, Lee M et al (2017) Optimizing the coupled effects of Hall-Petch and precipitation strengthening in a Al0.3CoCrFeNi high entropy alloy. Mater Des 121:254–260

[20] He JY, Wang H, Huang HL et al (2016) A precipitation-hardened high-entropy alloy with outstanding tensile properties. Acta Mater 102:187–196

[21] Xiaotao L, Wenbin L, Lijuan M et al (2016) Effect of boron on the microstructure, phase assemblage and wear properties of Al0.5CoCrCuFeNi high-entropy alloy. Rare Met Mater Eng 45:2201–2207

[22] Jiang H, Han K, Qiao D, et al (2018) Effects of Ta addition on the microstructures and mechanical properties of CoCrFeNi high entropy alloy. Mater Chem Phys 210:43–48

[23] Sun W, Huang X, Luo AA (2017) Phase formations in low density high entropy alloys. CALPHAD Comput Coupling Phase Diagr Thermochem 56:19–28

[24] Li C, Li JC, Zhao M, Jiang Q (2010) Effect of aluminum contents on microstructure and properties of AlxCoCrFeNi alloys. J Alloys Compd 504:S515–S518

[25] Wang W-R, Wang W-L, Wang S-C et al (2012) Effects of Al addition on the microstructure and mechanical property of AlxCoCrFeNi high-entropy alloys. Intermetallics 26:44–51

[26] Yurchenko NY, Stepanov ND, Shaysultanov DG et al (2016) Effect of Al content on structure and mechanical properties of the AlxCrNbTiVZr (x = 0; 0.25; 0.5; 1) high-entropy alloys. Mater Charact 121:125–134

[27] Tseng KK, Yang YC, Juan CC, et al (2018) A light-weight high-entropy alloy $Al_{20}Be_{20}Fe_{10}Si_{15}Ti_{35}$. Sci China Technol Sci 61:184–188

[28] Stepanov ND, Shaysultanov DG, Salishchev GA, Tikhonovsky MA (2015) Structure and mechanical properties of a light-weight AlNbTiV high entropy alloy. Mater Lett 142:153–155

[29] Hammond VH, Atwater MA, Darling KA et al (2014) Equal-channel angular extrusion of a low-density high-entropy alloy produced by high-energy cryogenic mechanical alloying. JOM 66:2021–2029

[30] Youssef KM, Zaddach AJ, Niu C et al (2014) A novel low-density, high-hardness, high-entropy alloy with close-packed single-phase nanocrystalline structures. Mater Res Lett 3:95–99

[31] Li R, Gao JC, Fan K (2010) Study to microstructure and mechanical properties of Mg containing high entropy alloys. Mater Sci Forum 650:265–271